AIP | Applied Physics Letters

Stress-induced growth of single-crystalline lead telluride nanowires and their thermoelectric transport properties

Dedi, Ping-Chung Lee, Chia-Hua Chien, Guang-Ping Dong, Wei-Chia Huang et al.

Citation: Appl. Phys. Lett. **103**, 023115 (2013); doi: 10.1063/1.4813606
View online: http://dx.doi.org/10.1063/1.4813606
View Table of Contents: http://apl.aip.org/resource/1/APPLAB/v103/i2
Published by the AIP Publishing LLC.

Stress-induced growth of single-crystalline lead telluride nanowires and their thermoelectric transport properties

Dedi,[1,2,3,a)] Ping-Chung Lee,[1,2,3] Chia-Hua Chien,[1,2,3] Guang-Ping Dong,[2,4] Wei-Chia Huang,[2] Cheng-Lung Chen,[2] Chuan-Ming Tseng,[2] Sergey R. Harutyunyan,[2,5] Chih-Hao Lee,[1] and Yang-Yuan Chen[2,4,a)]

[1]*Department of Engineering and System Science, National Tsing Hua University, Hsinchu 300, Taiwan*
[2]*Institute of Physics, Academia Sinica, Taipei 11529, Taiwan*
[3]*Nano Science and Technology Program, Taiwan International Graduate Program, Institute of Physics, Academia Sinica, Taipei 11529, Taiwan*
[4]*Graduate Institute of Applied Physics, National Chengchi University, Taipei 106, Taiwan*
[5]*Institute for Physical Research, NAS, Ashtarak-2, Armenia*

(Received 10 May 2013; accepted 25 June 2013; published online 12 July 2013)

Uniform single-crystal lead telluride (PbTe) nanowires (NWs) were synthesized using a stress-induced method, which is an alternative technique for synthesizing PbTe NWs without a catalyst. The thermoelectrical transport measurement of a NW with a diameter of 217 nm exhibited a notable enhancement over the room-temperature thermopower of $-342\,\mu V\,K^{-1}$, which was approximately 95% larger than the bulk of PbTe. The power factor of $104\,\mu W\,m^{-1}\,K^{-2}$ is also higher than any previously reported power factor in PbTe NWs. © *2013 AIP Publishing LLC*. [http://dx.doi.org/10.1063/1.4813606]

Growing novel nanowires is a crucial topic in nanoscience and nanotechnology research.[1–3] It is believed that the quantum size and confinement effects in one-dimensional (1D) nanowires (NWs) play crucial roles in enhanced thermoelectric performance. The efficiency of thermoelectric materials is determined by the dimensionless figure of merit *ZT*, which is defined as $S^2\sigma T/(\kappa_e + \kappa_l)$, where *S* is the thermopower or Seebeck coefficient, σ is the electrical conductivity, κ_e is the electronic thermal conductivity, and κ_l is the lattice-phonon thermal conductivity. This concept is related to Slack's proposal of a phonon-glass/electron-crystal (PGEC) model, which suggests that an efficient thermoelectric material has the electronic properties of a crystalline material and the thermal properties of a glass.[4] By properly adjusting the parameters for *S*, σ, and κ, the figure-of-merit *ZT* is enhanced.

The reduction of dimensionality from three dimensional (3D) to 1D results in a dramatic increase in the electronic density of states (DOS) at energy band edges, which in turn leads to an increase of the thermoelectric power factor ($S^2\sigma$). Therefore, the increased DOS of a 1D structure produces an enhanced $S^2\sigma$, and consequently, an enhanced ZT.[5,6] In NWs composed of thermoelectric materials such as PbTe, the nanometer scale is predicted to increase the *S*.[7,8] Based on certain carrier-scattering assumptions, the enhanced *S* occurs because of a sharp increase in the local DOS around the Fermi level, which is also interpreted as an increased local DOS effective mass (m_d*). However, the overall benefit of such an increase in *S* can be compensated by a decrease in carrier mobility μ, because the increased local DOS usually leads to a heavier transport-effective mass of carriers. In the most well-known high-temperature thermoelectrics, the carriers are predominantly scattered by phonons.[9] Increasing the *S* is an obvious goal for obtaining high efficiency thermoelectric materials, but other changes in transport properties often sacrifice the σ correlated with an increase in the *S* and do not ultimately lead to an improvement in *ZT*.

Lead telluride (PbTe) is a semiconductor with an energy band gap of 0.31 eV at 300 K that can be applied in mid-infrared lasers,[10–12] optical detectors,[13–15] and thermoelectricity.[16–18] The synthesis of low-dimensional PbTe materials such as nanowires[19–27] has been intensively studied in the past decades. A variety of methods have been used to synthesize PbTe NWs, such as the laser ablation method,[19] the chemical vapor transport method (CVT),[20,21] lithographically patterned nanowire electrodeposition,[22,23] potentiostatical electrodeposition using a track-etched polycarbonate membrane,[24] hydrothermal method,[25,26] and the simple one-step solvothermal polyol process.[27]

In 2002, Cheng *et al*. reported a stress-induced method used to grow Bi NWs from Bi-CrN composite thin film; it exploited the residual compressive stress in composite thin films as the driving force for NW formation. They predicted that this technique may also be suitable for growing NWs made of other materials.[28] More recently, Lee *et al*. proposed the fabrication of single-crystalline Bi and Bi_2Te_3 NWs based on a mechanism in which the mismatch of the thermal expansion between the substrate and the film drove the mass flow along grain boundaries to grow NWs at thermal annealing temperatures. This NW growth method, which does not involve using conventional templates, catalysts, or starting materials, has the advantage of controlling the growth conditions for the diameter, shape and aspect ratio of single-crystalline NWs.[29,30] This technique had not been previously applied to PbTe alloys. We applied the stress-induced method to grow single-crystalline PbTe NWs from PbTe thin film on a SiO_2/Si substrate without using a catalyst, enhancing the thermoelectric properties of the NWs.

[a)]Authors to whom correspondence should be addressed. Electronic addresses: dediamada@phys.sinica.edu.tw (Tel.: +886 2 2789 8401) and cheny2@phys.sinica.edu.tw (Tel.: +886 2 2789 6725; Fax: +886 2 2789 6725).

The films were prepared in a pulsed laser deposition (PLD) system (LPX Pro 210). The PbTe for the PLD target was made by mixing elemental Pb (Alfa Aesar, −200 mesh, 99.9%) and Te (Alfa Aesar, −325 mesh, 99.999%) inside a carbon-coated silica tube, which was then evacuated to a base 10^{-6} Torr, sealed, slowly heated to 1000 °C over a period of 12 h, held at this temperature for 4 h, and then cooled to room temperature. The ingot was cut into a disc shape with a diameter of 10 mm by a diamond saw. The disc target was polished and ultrasonically cleaned in acetone and methanol before being placed on the target holder. Films were deposited on single-crystal SiO_2/Si (100) substrates. The substrates were ultrasonically cleaned in acetone and methanol and then rinsed with deionized water before their introduction into the vacuum chamber. The base pressure of the vacuum system was 5.0×10^{-7} Torr. The excimer laser was applied at 140 mJ at a frequency of 10 Hz during a 15-min deposition at room temperature. The substrate rotation speed was approximately 10 rpm. The total thickness of the films was 20 nm. The deposition rate was approximately 0.22 Å s^{-1}, which was slower than the deposition rate for growing Bi/Bi_2Te_3 NWs[29,30] because of the differing thermodynamic properties of these compounds and the high melting point (T_m = 924 °C) of PbTe. The films were sealed in a vacuumed quartz tube below 5×10^{-6} Torr, annealed at 450 °C for 5 d, and then cooled to room temperature in the furnace. During the annealing process, the NWs grew from the film to release the compressive stress caused by the difference in thermal expansion coefficients between the PbTe film (19.8×10^{-6}/°C) and the SiO_2/Si substrate (0.5×10^{-6}/°C)/(2.4×10^{-6}/°C). Fig. 1(a) is a schematic diagram of the growth mechanism of PbTe NWs from PbTe thin film on a SiO_2/Si substrate. Annealing for 5 h at 450 °C produced short NWs, which were approximately 10 μm or less in length. Therefore, these NWs could not be placed on a microchip because the width of the window of a microchip is approximately 15 μm.

Scanning electron microscope (SEM) images of PbTe NWs with diameters ranging from 50 to 300 nm and lengths as high as several micrometers are shown in Fig. 1(b). Straight, uniform PbTe NWs with a high aspect ratio grew on the substrate after annealing. A tungsten needle (d_w = 100 nm) and a binocular optical microscope were used to pick a single NW from the PbTe thin film and place it on a Si_3N_4 microchip, on which the PbTe NW was suspended by electrodes. The microchip [Fig. 1(c)] was then used for structural analysis and thermoelectrical measurements of the crystal. A transmission electron microscope (TEM) was used to investigate the crystalline structure of PbTe NWs with diameters of 75 and 217 nm [Figs. 1(d) and 1(e)]. The TEM image and a corresponding selected-area electron diffraction (SAED) pattern revealed that the PbTe NWs were high-quality single crystals with a growth along the [100] direction. The lattice fringes of the smooth PbTe that were separated by 0.33 nm are consistent with a periodicity along the [200] direction with lattice constants of approximately 6.549 Å, which are approximately 1.2% higher than that of the bulk (a = 6.47 Å).

The chemical composition of the PbTe NWs was studied by using energy dispersive X-ray spectroscopy (EDS). The EDS line scan profile, shown in Figs. 2(a) and 2(d), revealed the uniform spatial distribution of the Pb and Te elements throughout the NW. This was further confirmed by using a

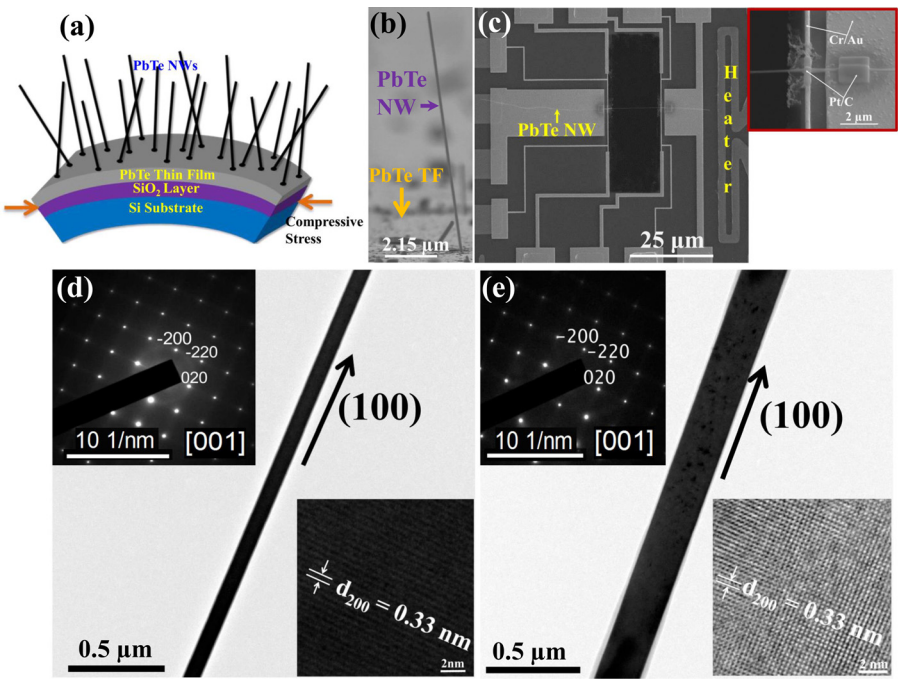

FIG. 1. (a) A representation of the growth mechanism in PbTe NWs using the catalyst-free stress-induced method. (b) An SEM image from above shows that all of the PbTe NWs grow several micrometers in length from the surface of the PbTe thin film. (c) The SEM images of a PbTe NW with a diameter of 75 nm suspended on a Si_3N_4 template after electrode formation by using a focus ion beam (FIB). The inset shows the Pt/C thermal contact between the PbTe NW and 10-nm Cr/50-nm Au electrodes on a Si3N4 microchip. After using the FIB, the contact resistance with the Pt/C was approximately 425–430 Ω. (d) Low-magnification TEM images of a PbTe NW with a diameter of 75 nm. The inset of the top left figure shows the SAED pattern (at the [001] zone axis), confirming that the single-crystalline NWs grew in the [100] direction. The inset of the bottom right figure shows a high-resolution TEM image of a PbTe NW with a diameter of 75 nm. The distance between crystal faces is 0.33 nm, indicating the [200] direction lattice fringes. (e) Low-magnification TEM images of a PbTe NW with a diameter of 217 nm shows a similar structure to a 75-nm NW.

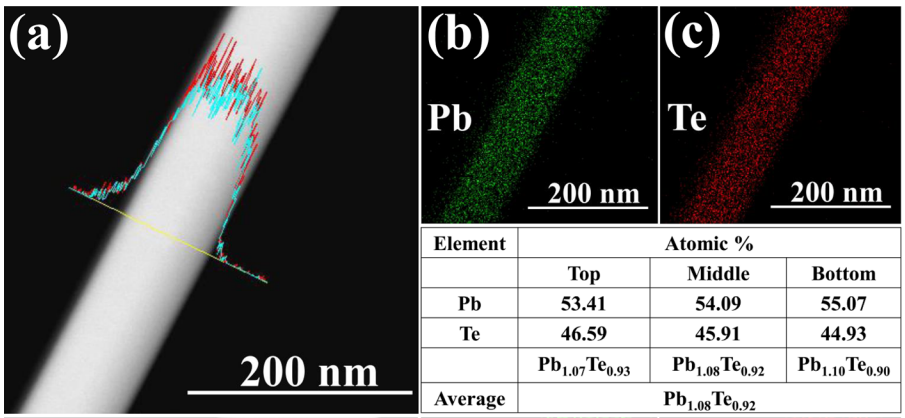

Element	Atomic %		
	Top	Middle	Bottom
Pb	53.41	54.09	55.07
Te	46.59	45.91	44.93
	$Pb_{1.07}Te_{0.93}$	$Pb_{1.08}Te_{0.92}$	$Pb_{1.10}Te_{0.90}$
Average	$Pb_{1.08}Te_{0.92}$		

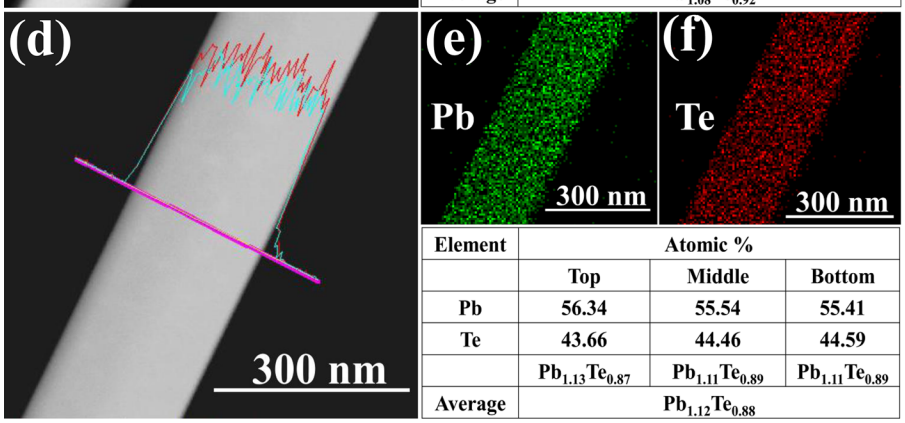

Element	Atomic %		
	Top	Middle	Bottom
Pb	56.34	55.54	55.41
Te	43.66	44.46	44.59
	$Pb_{1.13}Te_{0.87}$	$Pb_{1.11}Te_{0.89}$	$Pb_{1.11}Te_{0.89}$
Average	$Pb_{1.12}Te_{0.88}$		

FIG. 2. (a) and (d) STEM images of 75-nm and 217-nm PbTe NWs. The line profiles show that the Pb (blue line) and Te (red line) are homogeneously distributed throughout the NWs. (b), (c), (e), and (f) Elemental mapping showing the uniform distribution of Pb and Te along the length of 75-nm and 217-nm NWs, respectively.

scanning transmission electron microscope (STEM) to map elements across the NW [Figs. 2(b)–2(f)]. The EDS point scanning experiments of the NWs quantitatively confirm that Pb and Te are present in an average atomic ratio of 54.98% and 45.02%, respectively. The EDS data showed that the atomic ratio of Pb/Te ≈ 1.22 without any impurities. The stoichiometric composition of the individual NW was $Pb_{1.1}Te_{0.9}$.

Figure 3(a) shows the temperature dependence of the measured resistivities ρ, which exhibit a semiconducting behavior. The resistivities at near room temperature are $1.12 \times 10^{-3}\,\Omega\,m$ for the 217-nm NW, and $6.55 \times 10^{-4}\,\Omega\,m$

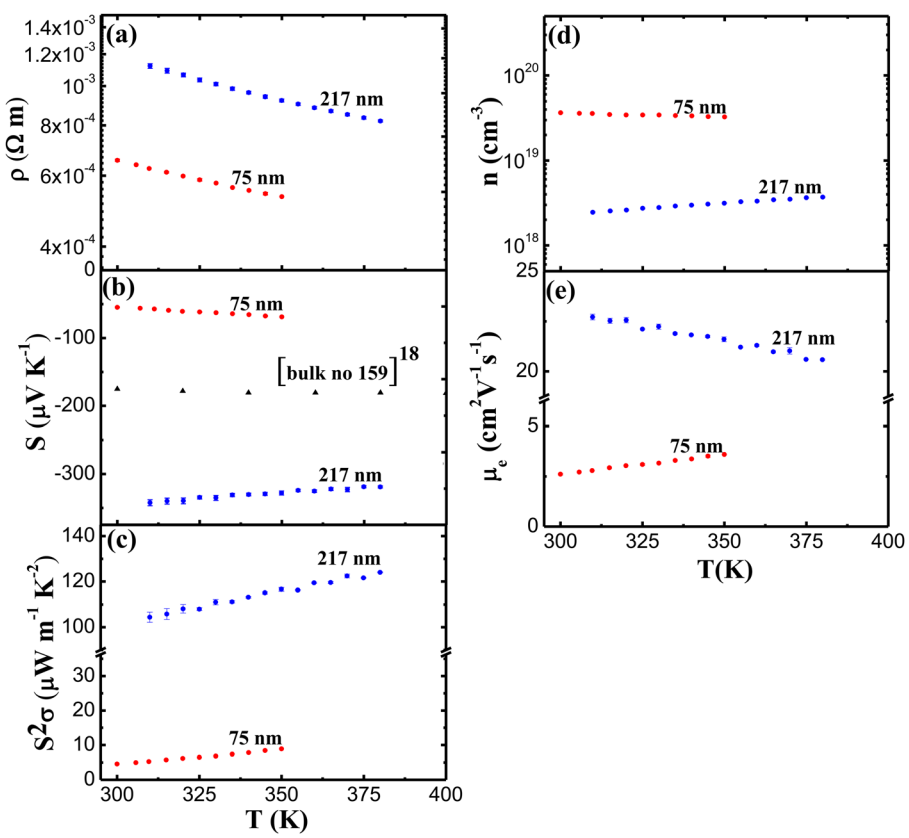

FIG. 3. Temperature dependence of (a) electrical resistivities, (b) thermopower, (c) power factor, (d) carrier concentration, and (e) carrier mobility for PbTe NWs with $d_w = 75$ nm and 217 nm.

for the 75-nm NW, which are 74 and 43 times greater than that of the PbTe bulk ($1.52 \times 10^{-5}\,\Omega\,m$).[18] An enhanced ρ probably arises from the surface scattering of charge carriers.[31]

The obtained S of PbTe NWs with the negative sign [Fig. 3(b)] shows that the PbTe NWs are n-type semiconductors because their electrons have a much higher μ than holes and dominate the electronic transport properties,[32,33] and that the S is controlled by electron diffusion. The S value obtained for the 217-nm NW represents the highest value of $-342.28\,\mu V\,K^{-1}$ at 310 K, which is approximately a 95% enhancement over the $-175\,\mu V\ K^{-1}$ of the corresponding n-type PbTe bulk.[18] This results in a large enhancement of the thermo power, S in comparison with the bulk sample because of an increase in the DOS of electrons near the Fermi level in the NWs.[8,22,25,34] The effect of this local increase in DOS on S is given by the Mott expression[34]

$$S = \frac{\pi^2}{3}\frac{k_B}{q}k_BT\left\{\frac{d[\ln(\sigma(E))]}{dE}\right\}_{E=E_F} = \frac{\pi^2}{3}\frac{k_B}{q}k_BT\left\{\frac{1}{n}\frac{dn(E)}{dE}+\frac{1}{\mu}\frac{d\mu(E)}{dE}\right\}_{E=E_F.} \quad (1)$$

Here, S depends on the energy derived from the energy-dependent electrical conductivity $\sigma(E) = \sigma(E)q\mu(E)$ taken at the Fermy energy (E_F), when $n(E) = g(E)f(E)$, and the carrier density at energy level E is considered, where f(E) is the Fermi function, q is the carrier charge, and $\mu(E)$ is the mobility. In contrast, the S of the 75-nm NW was $-54.76\,\mu V\ K^{-1}$ at 300 K, which is a relatively low value (less than 69% of that of the bulk).[18] These results are considered the consequences of structural imperfections, such as antisite defects caused by Pb_{Te} (i.e., the creation of one vacancy at the tellurium site), facilitate enhancing the carrier concentration.[18,35] The ρ was closely correlated with the S, which was consistent with samples in which a smaller ρ had a lower S value.

The σ value was derived from an experimental measurement of ρ; thus, at approximately 310 K the $S^2\sigma$ values were 4.58 and $104.38\,\mu W\,m^{-1}\,K^{-2}$ for 75-nm and 217-nm NWs, respectively. The $S^2\sigma$ values of PbTe NWs as a function of temperature are plotted in Fig. 3(c). The power factor decreased gradually when the temperature decreased, and the results were mainly attributed to the ρ trends of PbTe NWs. All measurements were conducted in a high vacuum of less than 2×10^{-6} Torr to eliminate convectional heat loss. The results are shown in Table I, along with literature values for NWs, nanowire film (NWF), and bulk PbTe.

According to alternative form of the Mott relation,[36] the carrier concentration n can be estimated from thermopower data by using

$$S = \frac{8\pi^2 k_B^2 T}{3qh^2} m_d^* \left(\frac{\pi}{3n}\right)^{\frac{2}{3}}, \quad (2)$$

with

$$g(E) = \frac{(m_d^*)^{3/2}\sqrt{2E}}{\hbar^3\pi^2}, \quad (3)$$

where k_B is the Boltzmann's constant, m_d* is the effective mass of carrier ($m_d^* = 0.30\,m_o$ in PbTe),[37] m_o is the electron mass, q is the electron charge, h is Planck's constant, T is the measurement temperature and g(E) is the density of states (DOS). The equation is valid for degenerate semiconductors having an n value in the range of 10^{18} to $10^{20}\,cm^{-3}$.[35,38] The n is approximately $3.27–3.65 \times 10^{19}\,cm^{-3}$ at 300–350 K for the 75-nm NW. For the 217-nm NW, the n is approximately $2.45–3.70 \times 10^{18}\,cm^{-3}$ at $T = 310–380$ K, indicating that the NWs are degenerate semiconductors. The temperature dependences of the n of the NWs are presented in Fig. 3(d). The number of carriers increased for the 217-nm NW when the temperature increased. Such behavior is the result of the generation of new carriers as the temperature increased. For the 75-nm diameter nanowire, n was relatively flat over a wide range of temperatures, indicative of extrinsic doping. The value of n and its behavior confirms that, even with the same composition (Pb/Te atomic ratio), the actual n may differ because of nanostructural and quality differences. The S was closely correlated with the n, which was consistent with samples in which a smaller n had a higher S value.[18]

Our calculated μ values were 2.61–3.59 $cm^2\,V^{-1}\,s^{-1}$ for the 75-nm NW and 20.60–22.70 $cm^2\,V^{-1}\,s^{-1}$ for the 217-nm NW. The μ value is obtained using the equation

$$\mu = \frac{1}{\rho nq} = \frac{\sigma}{nq}. \quad (4)$$

TABLE I. Summary of thermopower S, electrical conductivity σ, and power factor $S^2\sigma$ for nanowires, nanowire film, and bulk PbTe, measured at ~300 K.

Sample[a]	Size[b]	Carrier type	S ($\mu V\,K^{-1}$)	σ ($S\,m^{-1}$)	$S^2\sigma$ ($\mu W\,m^{-1}\,K^{-2}$)	Reference
SI (NW, SC)	217 nm × 13.65 μm	n	−342.28	890.90	104.38	This work
SI (NW, SC)	75 nm × 16.39 μm	n	−54.76	1526.19	4.58	This work
LPNE (NWA,PC)	60 nm × 200 nm × 200 μm (Grain diameter:10 ± 2)	n	−41	8100 ± 1800	14	22
CVT (NW, SC)	60 nm × 1.8 μm	n	−72	0.44	0.0023	21
TSHT (NWF, SC)	30 nm × 100 μm	n	−628	133.51	52.65	25
TSHT(NWF, SC)	20–40 nm × 100 μm	n	−307	273	26	26
Bulk ($Pb_{1.06}Te$ PC) No 159	30−60 nm (Grain diameter)	n	−175	65789.47	2014.80	18

[a]Abbreviation: SI = stress-induced, LPNE = lithographically patterned nanowire electrodeposition, CVT = chemical vapor transport, TSHT = two step hydrothermal, NW = nanowire, NWA = nanowire array, NWF = nanowire film, SC = single-crystalline, PC = polycrystalline.
[b]Diameter × length or width × height × length.

These values were much smaller than those of the PbTe bulk (approximately $209\,cm^2\,V^{-1}\,s^{-1}$),[18] but higher than the values of $0.7\,cm^2\,V^{-1}\,s^{-1}$, $0.83\,cm^2\,V^{-1}\,s^{-1}$, and $10\,cm^2\,V^{-1}\,s^{-1}$ estimated by Fardy *et al.*,[20] Jang *et al.*,[21] and Yang *et al.*,[22] respectively. The calculated T dependences of μ for PbTe NWs are depicted in Fig. 3(e). The main factor for determining μ in the semiconductor is the scattering processes. The actual mobility is $1/\mu = \Sigma 1/\mu_i$, where μ_i is mobility corresponding to a certain source of scattering. In the middle range of temperatures, the vital sources of scattering are the ionized impurities and phonons

$$\mu_i \propto (m_d^*)^{-\frac{1}{2}} N_I^{-1} T^{3/2}, \tag{5}$$

$$\mu_l \propto (m_d^*)^{-\frac{5}{2}} T^{-3/2}, \tag{6}$$

where N_I is the total ionized impurity density in the semiconductor.[12] The μ values of the 217-nm NWs show a continuous decrease with an increasing T, indicating that phonon scattering is dominant throughout the entire T range, whereas ionized impurity scattering is dominant in 75-nm NWs.

In summary, the stress-induced method was applied to grow individual single-crystal PbTe NWs from a PbTe thin film on a SiO_2/Si substrate, offering an alternative technique for PbTe NW synthesis without catalyst. This technique had not been previously applied to PbTe alloys. The $S(T)$ and $\rho(T)$ for 75-nm and 217-nm NWs were measured, and the temperature dependences of thermoelectrical power factors, carrier concentration, and mobility at 300–380 K were reported. The 217-nm NW exhibited the highest thermopower value, S, of $-342\,\mu V\,K^{-1}$ at 310 K, which is approximately a 95% enhancement over the reported value of the PbTe bulk.[18]

This work was supported by the National Science Council in Taiwan, under Grant No. NSC 100-2112-M-001-019-MY3. Technical support was provided by the Core Facilities for Nanoscience and Nanotechnology at the Academia Sinica in Taiwan.

[1]Y. Xia, P. Yang, Y. Sun, Y. Wu, B. Mayers, B. Gates, Y. Yin, F. Kim, and H. Yan, Adv. Mater. **15**, 353 (2003).
[2]N. Wang, Y. Cai, and R. Q. Zhang, Mater. Sci. Eng. R **60**, 1 (2008).
[3]Z. Li, Q. Sun, X. D. Yao, Z. H. Zhu, and G. Q. (Max) Lu, J. Mater. Chem. **22**, 22821 (2012).
[4]G. A. Slack, *CRC Handbook of Thermoelectrics* (CRC Press, Boca Raton, FL, USA, 1995).
[5]G. D. Mahan, Solid State Phys. **51**, 81 (1997).
[6]Y. Lin, X. Sun, and M. S. Dresselhaus, Phys. Rev. B **62**, 4610 (2000).
[7]L. D. Hicks and M. S. Dresselhaus, Phys. Rev. B **47**, 12727 (1993).
[8]L. D. Hicks and M. S. Dresselhaus, Phys. Rev. B **47**, 16631 (1993).
[9]Y. Pei, H. Wang, Z. M. Gibbs, A. D. LaLonde, and G. J. Snyder, NPG Asia Mater. **4**, e28 (2012).
[10]G. Springholz, T. Schwarzl, M. Aigle, H. Pascher, and W. Heiss, Appl. Phys. Lett. **76**, 1807 (2000).
[11]T. Schwarzl, W. Heiss, G. Springholz, M. Aigle, and H. Pascher, Electron. Lett. **36**, 322 (2000).
[12]S. M. Sze and K. K. Ng, *Physics of Semiconductor Devices*, 3rd ed. (Wiley-Interscience, Hoboken, NJ, 2007).
[13]C. Boschetti, I. Bandeira, H. Closs, A. Ueta, P. Rappl, P. Motisuke, and E. Abramof, Infrared Phys. Technol. **42**, 91(2001).
[14]A. Barros, E. Abramof, and P. Rappl, J. Appl. Phys. **99**, 024904 (2006).
[15]D. M. Rowe, *CRC Handbook of Thermoelectrics* (CRC Press, Boca Raton, FL, USA 1995).
[16]Z. Dughaish, Phys. B: Condens. Matter. **322**, 205 (2002).
[17]J. P. Heremans, C. Thrush, and D. Morelli, Phys. Rev. B **70**, 115334 (2004).
[18]J. P. Heremans, C. Thrush, and D. Morelli, J. Appl. Phys. **98**, 063703 (2005).
[19]Q. Wei and C. M. Lieber, Mater. Res. Soc. Symp. Proc. **581**, 219 (1999).
[20]M. Fardy, A. I. Hochbaum, J. Goldberger, M. M. Zhang, and P. Yang, Adv. Mater. **19**, 3047 (2007).
[21]S. Y. Jang, H. S. Kim, J. Park, M. Jung, J. Kim, S. H. Lee, J. W. Roh, and W. Lee, Nanotechnology **20**, 415204 (2009).
[22]Y. Yang, D. K. Taggart, M. H. Cheng, J. C. Hemminger, and R. M. Penner, J. Phys. Chem. Lett. **1**, 3004 (2010).
[23]Y. Yang, S. C. Kung, D. K. Taggart, C. Xiang, F. Yang, M. A. Brown, A. G. Guell, T. J. Kruse, J. C. Hemminger, and R. M. Penner, Nano Lett. **8**, 2447 (2008).
[24]H. Jung, D. Y. Park, F. Xiao, K. H. Lee, L. H. Choa, B. Yoo, and N. V. Myung, J. Phys. Chem. C **115**, 2993 (2011).
[25]G. Tai, B. Zhou, and W. Guo, J. Phys. Chem. C **112**, 11314 (2008).
[26]G. Tai, W. Guo, and Z. Zhang, Cryst. Growth Des. **8**, 2906 (2008).
[27]Q. Yan, H. Chen, W. Zhou, H. H. Hng, F. Y. C. Boey, and J. Ma, Chem. Mater. **20**, 6298 (2008).
[28]Y. T. Cheng, A. M. Weiner, C. A. Wong, M. P. Balogh, and M. J. Lukitsch, App. Phys. Lett. **81**, 3248 (2002).
[29]W. Shim, J. Ham, K. I. Lee, W. Y. Jeung, M. Johnson, and W. Lee, Nano Lett. **9**, 18 (2009).
[30]J. Ham, W. Shim, D. H. Kim, S. Lee, J. Roh, S. W. Sohn, K. H. Oh, P. W. Voorhees, and W. Lee, Nano Lett. **9**, 2867 (2009).
[31]D. Wang, B. A. Sheriff, and J. R. Heath, Small **2**, 1153 (2006).
[32]D. L. Partin, J. Heremans, D. T. Morelli, C. M. Thrush, C. H. Olk, and T. A. Perry, Phys. Rev. B **38**, 3818 (1988).
[33]A. H. Dekuijper and J. Bisschop, Thin Solid Films **110**, 99 (1983).
[34]J. P. Heremans, V. Jovovic, E. S. Toberer, A. Saramat, K. Kurosaki, A. Charoenphakdee, S. Yamanaka, and G. J. Snyder, Science **321**, 554 (2008).
[35]J. Horak, J. Navratil, and Z. Stary, Phys. Chem. Solids **53**, 1067(1992).
[36]G. J. Snyder and E. S. Toberer, Nature Mater. **7**, 105 (2008).
[37]H. A. Lyden, Phys. Rev. **135**, A514 (1964).
[38]C. H. Lee, G. C. Yi, Y. M. Zuev, and P. Kim, Appl. Phys. Lett. **94**, 022106 (2009).